Dissociative ionization of H_2, N_2, and O_2 by electron impact

B. Van Zyl and T. M. Stephen
Department of Physics, University of Denver, Denver, Colorado 80208
(Received 28 April 1994)

The data obtained by Rapp, Englander-Golden, and Briglia [J. Chem. Phys. **42**, 4081 (1965)] on the dissociative-ionization fractions and cross sections for electron impact on H_2, N_2, and O_2 molecules have been reanalyzed. Trajectories of the atomic ions produced in the crossed electric and magnetic fields within their target cell were computed as functions of ion energy and angular distribution, leading to a determination of how their ion-collection efficiencies depended on these parameters. Relative ion-energy and angular distributions as functions of incident electron energy from a variety of experimental studies were then incorporated into the calculations to yield total collection efficiencies, to be compared with the value of 40% estimated during the original measurements. For 100-eV electrons, the comparisons indicate that the reported dissociative-ionization fractions and cross sections should be increased by about 15% for N_2 and O_2 targets, but by almost 70% for H_2 targets, with all corrections increasing markedly at lower electron energies.

PACS number(s): 34.80.Gs

I. INTRODUCTION

In describing their technique for studying dissociative ionization of molecules by electron impact, Rapp, Englander-Golden, and Briglia [1] state that "Although the results are not expected to be extremely accurate, they give the correct magnitude, and are presented in the absence of results from a more precise method at this time." In spite of this qualifying remark, many workers have granted these approximate results a similar high stature to that justifiably given to the total ionization cross-section measurements reported by Rapp and Englander-Golden [2]. This is probably because no "more precise method" has evolved over the intervening years.

The reason these data were regarded as approximate was not associated with any inferior measurements of the electron-beam or target-gas-density magnitudes. Indeed, these parameters were determined quite carefully [2]. Rather, the problem resulted from an unknown collection efficiency for the atomic ions under study, an efficiency depending not only on the (ion-retarding) electric field and (electron-beam-collimating) magnetic field present in the interaction region, but also on the kinetic-energy and angular distributions of the ions themselves. Under the assumptions that the atomic-ion dissociation energy was much larger than the retarding potential applied to the ion collector, and that the ion angular distribution was not highly anisotropic, Rapp, Englander-Golden, and Briglia [1] deduced a total-ion-collection efficiency of about 40% from geometrical considerations of their target-cell configuration.

While more detailed ion-collection-efficiency calculations, including the effects of initial ion kinetic energy and angular distribution, would have been rather time consuming 30 years ago, they pose no real problem today. We thus decided to reanalyze these otherwise accurate results for dissociative ionization by including fragment ion energies between 0 and 15 eV and various angular distributions. Section II describes our calculations and their influence on the Rapp, Englander-Golden, and Briglia [1] measurements.

While these results should be quite definitive, they are of little value without some knowledge of the initial kinetic-energy and angular distributions of the dissociating ionic fragments. In general, the available data on these distributions are quite limited and sometimes contradictory, making an exact correction to the Rapp, Englander-Golden, and Briglia [1] data impossible. However, enough information is available for H_2, N_2, and O_2 molecules to piece together physically reasonable distributions to estimate corrections to these data. The way these distributions were obtained is described in Sec. III.

Section IV presents the results of our analyses, indicating the amounts we believe the dissociative-ionization fractions measured by Rapp, Englander-Golden, and Briglia [1] should be increased. Our results are compared with those of Krishnakumar and Srivastava [3–5], probably the most complete and reliable set of direct experimental data available at this time.

II. ION-COLLECTION-EFFICIENCY CALCULATIONS

The experimental configuration employed by Rapp, Englander-Golden, and Briglia [1] for their dissociative-ionization studies was a parallel-plate ionization chamber traversed by a magnetically confined (500 G) electron beam. The plate separation was 1.0 cm, their length (along the electron beam) was 6.5 cm, and their width (perpendicular to the electron beam) was 4.4 cm [6]. The ion collector itself was a (centered and electrically isolated) portion of one plate, about 1.8 cm long and 4.4 cm wide.

For their total ionization cross-section measurements, Rapp and Englander-Golden [2] applied a positive potential to the plate opposite the ion collector to drive positive ions to the collector surface. The applied potential

was sufficient to achieve a "saturation" of the collector current, independent of the initial ion kinetic energy and angular distribution of the dissociated-ion component of this current. In other words, the ion-collection efficiency for these measurements was unity.

In contrast, the ion collector was biased slightly positive (normally +0.25 V with respect to the electron-beam-axis potential) for the dissociative-ionization studies. This "retarding" potential prohibited any parent molecular ions (N_2^+, for example, assumed to be produced "at rest") from reaching the collector, but nevertheless allowed collection of a fraction of the atomic fragment ions with kinetic energies above 0.25 eV. It is this fraction and its dependence on the initial atomic-ion energy and dissociation angle that we will attempt to determine here.

Before proceeding, we should note that for H_2 (and D_2) targets, Rapp, Englander-Golden, and Briglia [1] used a ten-times larger ion-retarding field in their ionization chamber (with the collector plate at +2.5 V and the opposite plate at −2.5 V). This was done to prevent measurement of low-energy H^+ produced from transitions to the inner repulsive wall of the $H_2^+(^2\Sigma_g^+)$ ground-state potential-energy curve above its dissociation limit. Thus, only H^+ with kinetic energies in excess of 2.5 eV could be observed. This larger "kinetic-energy threshold" for ion observation should reduce the net collection efficiency to smaller values than for N_2 or O_2 targets.

The ion-collection calculations made here were straightforward in principle. Trajectories for ions produced along the target-cell (electron-beam) axis and moving under the influence of the applied electric and magnetic fields were determined analytically, with typical orbits being verified using SIMION software. At each ion energy, a trajectory defined by some combination of the polar (θ) and azimuthal (Φ) angles of an initial-ion-velocity vector relative to the target-cell axis was computed. The path length along this axis from which an originating ion could reach the ion collector was then determined, and compared with the total path length available to determine the ion-collection efficiency for this trajectory.

The relative contribution of this trajectory to the total ion-collection efficiency was estimated by assuming that all ion-angular distributions could be approximated by

$$I(\theta)=I(90°)[1+P\cos^2\theta]$$
$$=I(54.7°)\frac{[1+P\cos^2\theta]}{[1+P/3]}\ , \qquad (1)$$

where $I(90°)$ and $I(54.7°)$ are the atomic-ion intensities normal to, and at the magic angle relative to, the electron beam, and P is the "polarization" parameter. (While more complex distributions are possible [7,8], most of the experimental results we will consider in Sec. III can be fit approximately to this simple form.) Thus by "weighting" the trajectory calculated above by Eq. (1), appropriate summations over all similarly-computed trajectories (separated by 0.5° intervals in both θ and Φ) could be executed, yielding total ion-collection efficiencies as functions of polarization and initial ion energy.

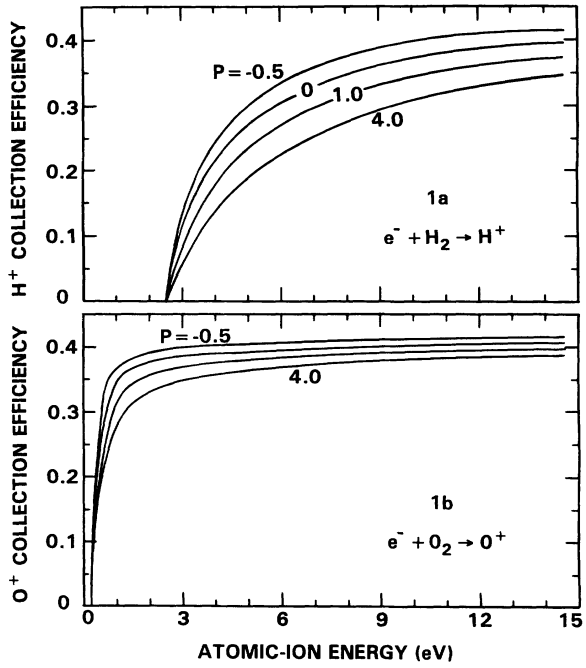

FIG. 1. Fragment ion-collection efficiencies versus ion energy and ion polarization for dissociative ionization of H_2 and O_2 by electron impact.

We show in Fig. 1 the resulting ion-collection efficiencies for H^+ and O^+ from dissociative ionization of H_2 and O_2 molecules for 0–15-eV ion energy and at the polarizations noted. (Data for N^+ from N_2 are not shown here, as they differ only slightly from the O^+ results at comparable ion energies.)

As can be seen, for O^+ from O_2, the ion-collection efficiencies do indeed approach about 40% at the higher ion energies, and their polarization dependence is not very strong, as correctly estimated by Rapp, Englander-Golden, and Briglia [1]. All efficiencies here remain fairly constant for O^+ energies down to a few eV, below which they drop off rapidly to zero at 0.25 eV as a result of the ion-collector-bias potential discussed above. For H^+ from H_2, however, the efficiencies drop off much faster with decreasing H^+ energy, their polarization dependence is much stronger, and their cutoff energy is larger (2.5 eV), all the result of the increased collector-bias potential applied for this species.

Note also that the ion-collection efficiencies for negative polarizations are larger, as expected for distributions peaking normal to the electron beam (and therefore toward the collector surface). However, as we will see below, most measured nonzero polarizations are positive, particularly for H_2, further reducing the ion-collection efficiencies for this species to well below the 40% value assumed by Rapp, Englander-Golden, and Briglia [1].

III. ION-ENERGY AND ANGULAR DISTRIBUTIONS

It would not be possible here to review all the available data on the ion-energy and angular distributions resulting

from the dissociative ionization of H_2, N_2, and O_2 by electron impact. However, this paper would be incomplete without at least a brief summary of the information used to generate the model distributions employed for our calculations. We present such a summary below, considering first the results for H_2 molecules.

We begin our summary with the studies of Dunn and Kieffer [9]. These workers identified the dominant feature of most ion-energy-distribution measurements at high electron and ion energies, a rather broad peak structure reaching a maximum near 8-eV H^+ energy. The source of these H^+ was thought to be direct ionization to the $^2\Sigma_u^+$ repulsive state of H_2^+, and calculations were made to show that this process would yield H^+ with about this energy.

The general form of this H^+ energy distribution was subsequently verified by Kieffer and Dunn [10] and by Köllmann [11]. During these studies, however, it became increasingly clear that this broad energy-distribution peak was composed of H^+ from more than one process. This point was dramatically illustrated later by Van Brunt [12], who showed the structure to be composed of two processes, one dominant at $\theta=90°$ and having its maximum at an H^+ energy near 5.2 eV, and the other dominating at small θ with its maximum between 7- and 8-eV H^+ energy. At intermediate angles, a "double-peaked" structure was observed, similar to the earlier findings for D_2 targets by Stockdale *et al.* [13].

Van Brunt and Kieffer [14] demonstrated that the relative magnitude of these two processes was electron-energy dependent, the process peaking near 5.2 eV becoming relatively smaller for electron energies below 100 eV. Data in that paper (see Fig. 3) also show the growth of a "high-energy tail" on the measured H^+ energy distributions with increasing electron energy, possibly from the dissociative ionization to higher excited states of H_2^+ (including $H^+ + H^+$), as had been suggested earlier [10].

Having identified three H^+ production processes so far, we temporarily interrupt our discussion to show how this information is incorporated into our ion-energy-distribution model. We show in Fig. 2 five normalized H^+-energy-distribution curves. Those peaks labeled 3, 4, and 5 represent our models for the processes described above. The peak 4 distribution, for example, with its maximum at 7.6-eV H^+ energy, is taken to be that for ionization to the $H_2^+(^2\Sigma_u^+)$ repulsive state. Its shape is from the theoretical calculations made by Kieffer and Dunn [10] (the dashed-line curve in their Fig. 1). The peak 5 distribution is roughly what might be expected from a similar calculation to the $H^+ + H^+$ state (and to highly excited H_2^+ Rydberg states just below it). We have no theoretical basis for the shape of peak 3, but it must be similar to that shown in order to simulate such experimental results as reported, for example, by Van Brunt [12] and Van Brunt and Kieffer [14].

Figure 2 also shows two other low-H^+-energy distributions to be discussed. Peak 1 is taken to represent H^+ from that portion of the ground-state $H_2^+(^2\Sigma_g^+)$ potential-energy curve lying above its dissociation limit

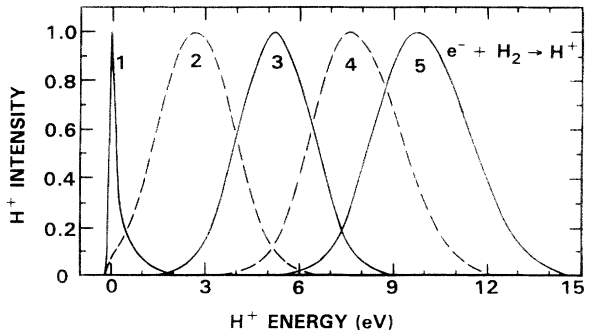

FIG. 2. H^+ energy distributions for the five H^+ production processes included in the computational model.

(at an internuclear separation close to 0.6 Å). The shape of this curve was basically taken from calculations by Dunn and Kieffer [9] (see their Fig. 1), although it was broadened slightly to show how it might appear if measured with an 0.1 eV-resolution detector. (We did this to facilitate comparison with the measured data of Locht *et al.* [15] and Locht and Schopman [16] for similar "zero-energy" peaks in the N^+ and O^+ energy distributions to be discussed later.)

The shapes of peaks 1, 3, 4, and 5 can thus all be traced to some theoretical or experimental finding. However, this is not true for peak 2. This peak is included here to represent the sum over some unknown number of "autoionizing" processes with thresholds from 22- to 28-eV electron energy, and giving H^+ with energies in the range of a few eV.

Unfortunately, the available data on these processes, too numerous to summarize here, are badly scattered, reflecting the difficulty of such studies. Köllmann [17] for example, claimed to see three such processes, while Landau, Hall, and Pichou [18] found five. Both measurements faced large energetic-ion-discrimination problems, but at least attempted to correct [18] (or indicate how to correct [17]) their results for such effects (which many workers appear to have just ignored). Fortunately, at low electron energies (≤ 30 eV), where few energetic H^+ are formed, both these studies found energy-distribution peaks with maxima near 2.7-eV H^+ energy (the basis for our peak 2 in Fig. 2).

As the electron energy was increased from 29 to 35 to 40 eV, this simulated peak 2 maximum remained an important feature in the energy distributions measured by Landau, Hall, and Pichou [18] [shown in their Fig. 4(b)], as seems reasonable to expect. In contrast, it is not present in the 40-eV H^+ energy distribution reported by Köllmann [17] after applying the recommended correction (shown in his Fig. 10), although it is present in the "raw data" (in his Fig. 3). We cannot explain this discrepancy. We should note, however, that these ($\theta=55°$) data of Landau, Hall, and Pichou [18] also seem to merge better with the (90°) results of Burrows *et al.* [19] at the lower electron energies, and with reasonable extrapolations of the higher-electron-energy data of Van Brunt and Kieffer [14] discussed above. For these

reasons, we have relied heavily on these results of Landau, Hall, and Pichou [18] at the lower electron energies in our modeling of the needed H^+ energy distributions.

This modeling consisted initially of adjusting the relative intensity of each of the individual H^+-energy-distribution peaks in Fig. 2 so that their sum reasonably duplicated a measured result at some electron energy and angle. This could not be done uniquely, of course, for Eq. (1) shows that the intensity of each process $I(\theta)$ depends on both its "average intensity" $I(54.7°)$, and its polarization P. It was thus necessary to independently establish reasonable values for one of these parameters. We decided to so establish the polarization values, for considerable data are available to satisfy this requirement.

Again, the pioneering work of Dunn and Kieffer [9] provides for much of the data needed. These workers measured polarizations of the H^+ observed at H^+ energies of 11.8, 8.6, and 3.7 eV for 10 electron energies. As it turns out, most of the H^+ observed with 11.8-eV energy must come, in our model, from peak 5 (see Fig. 2). Also, we found that the intensity of peak 4 is always larger than peak 5, so that most of the H^+ measured near 8.6 eV must come from peak 4. Similarly, except at low electron energies, the peak 2 contributions to the 3.7-eV H^+ signal are quite small, so these data basically show the polarization of peak 3. Finally, both theory [20] and experiment [21] suggest that the polarization of H^+ from the peak 1 process should be zero.

The polarization data used in our calculations are shown in Fig. 3. As can be seen, the P_3, P_4, and P_5 values are remarkably similar to the data of Dunn and Kieffer [9] (in their Fig. 4) cited above. The results plotted for P_2 are again estimated from the measurements of Köllmann [17] and Landau, Hall, and Pichou [18] both of which give polarization data at electron energies below 30 eV (the latter actually reporting results on individual autoionizing processes, which show only minimal variation). These data seem to indicate that the net polarization of our peak 2 processes should be about 1.5 at these low electron energies, and should slowly decrease with increasing electron energies above this region. (For electron energies above 50 eV, the P_2 values used in our model are rather irrelevant, as the fraction of the H^+ from all peak 2 processes rapidly decreases at the higher electron energies.)

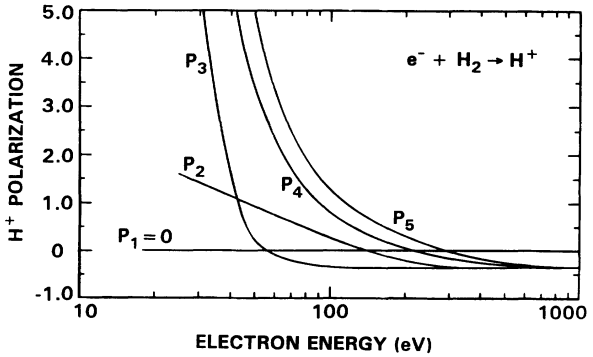

FIG. 3. H^+ polarizations for the five H^+ production processes included in the computational model.

We should note that the measured polarizations for dissociative ionization of H_2 by electron impact generally exhibit an asymmetric departure from the simple form of Eq. (1), with $I(\theta)$ being larger for $\theta < 90°$ than for $\theta > 90°$. This is usually attributed to momentum transfer from the electrons during the collisions, which also causes the H^+ energy distributions measured at $\theta > 90°$ to be shifted to slightly smaller H^+ energies [14]. We have ignored this forward-backward asymmetry by simply trying to "average" all polarization and energy-distribution data taken at $\pm$ angles about 90°. This approximation should be quite good except perhaps at the lowest electron energies, where the polarization asymmetries can be quite large [17,18].

The only other approximation made was to modify the shapes of the model H^+-energy-distribution curves in Fig. 2 at low electron energies. The high-H^+-energy sides of these distributions could be reduced gradually to zero (and, indeed, eventually the entire distribution) to insure that no H^+ would be counted at H^+ energies below their production threshold.

As a particularly nice example of how our model could reproduce experimentally-measured H^+ energy distributions, we present in Fig. 4 a comparison of our calculated results with the data of Van Brunt [12] for 75-eV electrons. Using the polarization data of Fig. 3 in Eq. (1), we adjusted the relative peak intensities in our model, $I(54.7°)$, to fit the (normalized) experimental results for $\theta = 23°$ shown in Fig. 4(a). Note that the fit is quite good, and that our calculated total distribution is slightly displaced from the data to lower H^+ energies, as expected from the influence of the forward-backward asymmetry effect noted above [14].

We then changed only our model " observation angle" to 90°, and generated the total H^+ energy distribution

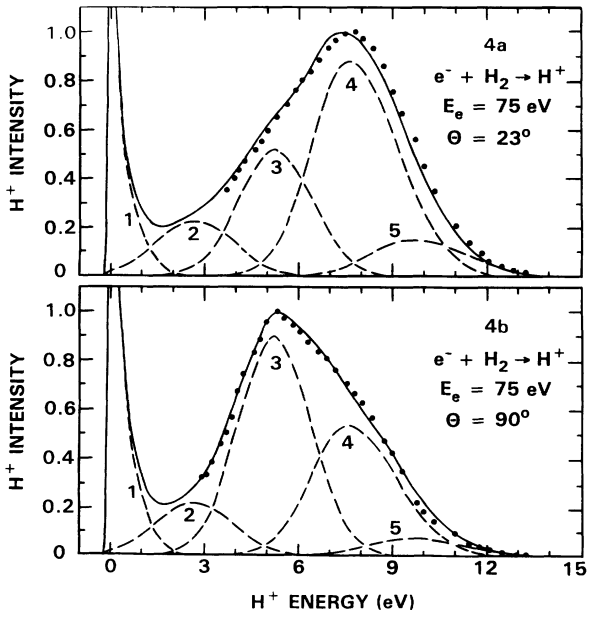

FIG. 4. Normalized H^+ energy distributions for dissociative ionization of H_2 by 75-eV electrons. The data points are from Van Brunt (Ref. [12]).

shown in Fig. 4(b). Obviously, the shape of the distribution is quite different, the contributions from peaks 4 and 5 being smaller because of their high positive polarizations. Nevertheless, a reasonable fit to the data of Van Brunt [12] is maintained, seemingly indicating that our interpretation of these results is basically correct.

Before ending this discussion of H_2 targets, we should note that, except for the original work of Köllmann [11], little information is available on the relative height of peak 1 to be used in such model H^+ energy distributions as shown in Fig. 4. However, because the source of these H^+ is the $H_2^+(^2\Sigma_g^+)$ potential-energy curve, the magnitude of this H^+ component should scale with the amount of H_2^+ produced in the collisions. A variety of procedures were used to estimate the appropriate "scale factor" for the production ratio of H^+ to H_2^+, i.e., $N(H^+)/N(H_2^+)$, including Franck-Condon-factor calculations [22–24] experimental [23,25] and theoretical [26,27] near-threshold photoionization studies, and the electron-impact measurements of Crowe and McConkey [21] at electron energies below 24 eV.

The end result of this analysis led us to believe that the ratio $N(H^+)/N(H_2^+)$ from this process should be about 0.0085 at 21-eV electron energy, increasing to 0.0135 at 24 eV (from the Crowe and McConkey [21] data), and given at the higher electron energies approximately by

$$\frac{N(H^+)}{N(H_2^+)} = \frac{0.020\,57[E_e - 19.0]}{\sum_v q_{0v}[E_e - E_t(v)]}, \tag{2}$$

where E_e is the electron energy, $E_t(v)$ is the ionization potential for producing H_2^+ in vibrational level v, and q_{0v} are Franck-Condon factors [24] for the $H_2(v=0) \rightarrow H_2^+(v)$ transition (but renormalized here to sum to $1.000\,00 - 0.020\,57 = 0.979\,43$). This expression gives the desired value of 0.021 in the high-electron-energy limit, and provides a suitable peak 1 normalization at all intermediate electron energies.

We now turn our attention to the available ion-energy- and angular-distribution data for dissociative ionization of N_2 and O_2. For electron energies above about 50 eV, such studies as made by Van Brunt and Kieffer [28] for N_2 and Van Brunt *et al.* [29] for O_2 show that the polarizations approach zero [30], which we initially thought would simplify our data-fitting procedures significantly. However, it soon became apparent that many more than five processes contributed to the measured N^+ and O^+ signals, easily overcoming any reduction in modeling effort resulting from the nonpolarized ion emission patterns. In fact, we found it necessary to incorporate a minimum of ten processes into our computational models for these molecules, even though we have little insight as to what physical mechanisms they represent.

At least for these molecules, we do have what appears to be reasonable high-resolution data for very-low-energy, atomic-ion production. For N_2 targets, the paper by Locht *et al.* [15] presents N^+-energy-distribution data for electron energies of 26, 28, 40, and 80 eV, all showing a pronounced (but very narrow) peak with its maximum at (or very close to) 0-eV N^+ energy. (This peak had been seen earlier by Köllmann [11], although with much reduced resolution.) For O_2 molecules, a similar situation occurs, as shown by the work of Locht and Schopman [16] at 60- and 35-eV electron energy, and at 25 eV by Schopman and Locht [31].

While the above data of Locht and colleagues [15,16,31] form the basis for our models of the ion-energy distributions at low ion energies, Locht *et al.* [15] note that the "closed structure of the ion source" is "responsible for a discrimination against highly energetic ions." To quantify this observation, they compare (in their Fig. 1) a measured N^+ energy distribution at 80-eV electron energy with that found at 75 eV by Köllmann [11], showing that their ion-collection efficiency did indeed decrease much faster above a few eV N^+ energy than did Köllmann's [11] (a problem actually underestimated by the differences in electron energy used).

A similar comparison can be made between the data of Locht and Schopman [16] and those of Van Brunt *et al.* [29] for O^+ from dissociative ionization of O_2 by 60-eV electrons, and is shown here in Fig. 5. The solid-line curve is the Locht and Schopman [16] result, and the dashed-line curve shows our estimate of how much this result must be increased (for ion energies above a few eV) to bring it into agreement with the data points of Van Brunt *et al.* [29]. The difference between these two curves can be explained by assuming the apparatus used by Locht and his colleagues [15,16,31] exhibited a (relative) ion-collection efficiency shown by the solid line in Fig. 6. (In other words, the dashed line in Fig. 5 was obtained by dividing the solid line in Fig. 5 by this efficiency.)

Unfortunately, this comparison of these O^+ data is not as straightforward as the above discussion would suggest, because some of the data points of Van Brunt *et al.* [29] plotted in Fig. 5 have also been adjusted. Their apparatus, in contrast to that used by Locht and colleagues

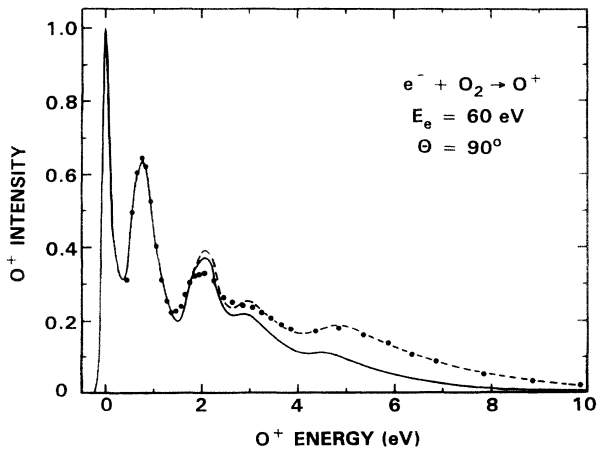

FIG. 5. O^+ energy distributions for dissociative ionization of O_2 by 60-eV electrons. The solid-line curve is the data of Locht and Schopman (Ref. [16]) and the dashed-line curve shows our estimated correction of these results. The data points are from Van Brunt *et al.* (Ref. [29]), adjusted here for O^+ energies below about 3 eV (see text).

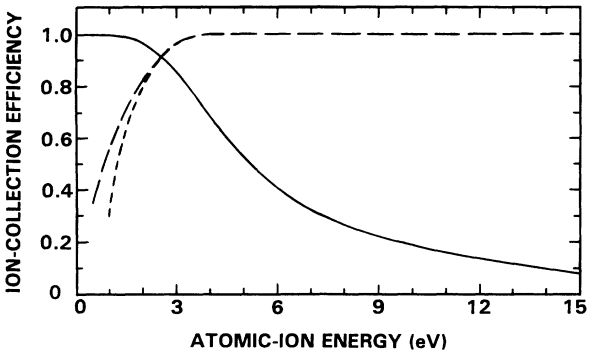

FIG. 6. Estimated ion-collection efficiencies used to correct experimental data for dissociative ionization of N_2 and O_2 by electron impact (see text).

[15,16,31], discriminated against low-energy ions (the reason why such H^+ energy distributions as shown in Fig. 4, for example, were not extended to ion energies below about 3 eV). Nevertheless, after careful comparisons of data similar to those shown in Fig. 5 at several electron energies for both N_2 and O_2 targets, we estimated that the ion-collection efficiency of this apparatus must be something like the dashed-line curves shown in Fig. 6. The upper long-dashed curve was thus used to raise the data of Van Brunt *et al.* [29] shown in Fig. 5 below about 3-eV O^+ energy, for these results were obtained using an "ion focusing" condition to "reduce ion discrimination at low kinetic energies." (Where this condition was not used, we recommend the correction indicated by the lower short-dashed curve.)

We should also note that the data of Van Brunt *et al.* [29] in Fig. 5 have been shifted to lower O^+ energies by 0.15 eV. Such shifts, generally between 0.05- and 0.15-eV ion energy, usually resulted in substantially better agreement with the data of Locht and colleagues [15,16,31] (and are within the ± 0.2-eV energy-scale uncertainty cited by Van Brunt and co-workers [28,29]). Furthermore, the influence of the energy-dependent resolution of Van Brunt's ion detector (wherein $\Delta E_i = 0.1 E_i$) is apparent in Fig. 5, where the resolution of the higher-energy O^+ structures is obviously diminished relative to that near the 0.8-eV O^+ peak.

Before leaving this discussion of Fig. 5, we point out that this net O^+ energy distribution shows distinct O^+ production processes reaching maxima at about 0, 0.85, 2.05, 3.00, and 4.85-eV O^+ energy. These are the peaks numbered 1, 3, 5, 7, and 8 in our computational model for O_2. Smaller and less apparent here (at this intermediate electron energy) are peaks 2, 4, and 6, which reach maxima near 0.45, 1.75, and 2.70-eV O^+ energy, and tend to be most important for duplicating similar measured O^+ spectra at low electron energies [29,31]. The two other peaks used, 9 and 10, which appear to have relatively high-electron-energy thresholds, reach maxima at about 6.55- and 8.70-eV O^+ energy, and are responsible for increasing the high-energy tail of the O^+ energy distributions at still large electron energies [29].

The situation is rather similar for N_2 targets. In addition to a large peak (1) at zero N^+ energy, nine others maximizing at 0.40, 0.65, 0.75, 1.20, 1.65, 2.35, 3.75, 5.60, and 8.90-eV N^+ energy were needed to reasonably duplicate the energy-distribution data of Locht *et al.* [15] and Van Brunt and Kieffer [28] (again after correcting these data for the ion-collection efficiencies shown in Fig. 6). Here peaks 3 and 6 were only important at low electron energies (similar to peaks 2, 4, and 6 for O_2), while peaks 9 and 10 were again included to fit the high-energy tails on the measured distributions at large electron energies [28,32].

Generally, the detailed shapes of the various peaks used in our model calculations for N_2 and O_2 targets are reasonably similar to those shown in Fig. 2 for H_2, and are not presented here. They are, however, available from the authors upon request.

While, as noted above, the polarizations of product N^+ and O^+ ions are near zero at electron energies above 50 eV [30], positive polarizations were measured [28,29] at lower electron energies and at selected ion energies above 0.95 eV. Curiously, we could approximately model these data by assuming that only peaks 3 and 6 yield polarized N^+ from N_2, and only peaks 2, 4, and 6 give polarized O^+ from O_2 (i.e., those peaks prominent in duplicating the measured ion-energy distributions at low electron energies). The values of the polarizations needed to fit the N_2 data (for peaks 3 and 6) started up near 50-eV electron energy, increasing to about 2.4 at 28 eV, with an electron-energy dependence rather like the P_3 curve in Fig. 3. For O^+ from O_2, the P_2, P_4, and P_6 polarizations were similar, but occurred at electron energies only 0.77 as large as for N^+ from N_2 (which value is in the approximate ratio of the dissociative-ionization thresholds for these species). Again, more detailed data are available upon request.

It appears that many of the low-energy N^+ and O^+ ions produced by electron impact on N_2 and O_2 result from predissociation of $N_2^+(C^2\Sigma_u^+)$ and $O_2^+(B^2\Sigma_g)$ molecular ions [15,16,28,29,31]. These reaction mechanisms and others leading to atomic-ion production are discussed in these references, and we recommend them for review.

In general, however, we have not tried seriously to assign physical mechanisms to the ten peaks used to model the measured ion-energy distributions for N_2 and O_2 targets. In fact, even the number of processes represented by these models is open to question. Some small peaks, for example, can be replaced with the addition of high-energy tails on lower-ion-energy peaks, with little influence on the overall ion-collection computations. For electron energies well above threshold, smaller and sharper peaks superimposed on broad underlying distributions can also be used to reasonably fit the measured data. Thus, the ten-peak models actually used for our calculations are certainly not unique, but nevertheless do a reasonable job of simulating the gross features of the available experimental data over an extended electron-energy range, the goal of this modeling effort.

IV. RESULTS AND DISCUSSION

Using the fragment-ion-energy and angular distributions established above, and the ion-collection efficiencies as functions of these parameters from Sec. II, we can now compute the fraction of the atomic ions produced that Rapp, Englander-Golden, and Briglia [1] would collect during their measurements. For example, for 75-eV electrons on H_2, the relative fractional areas under the ion-energy distributions in Fig. 4 at $\theta = 54.7°$ are 0.176, 0.104, 0.305, 0.345, and 0.061 for peaks 1–5, respectively. (At this "magic angle" where all polarization effects are averaged out, these areas should be proportional to the relative cross sections for dissociative ionization via these processes.) The corresponding polarizations are 0, 0.31, −0.23, 1.80, and 2.49 from Fig. 3. Using these distributions, we calculate that none of the very-low-energy H^+ under peak 1 would be collected, only 0.081 of those under peak 2, and 0.276, 0.292, and 0.314 of those H^+ under peaks 3, 4, and 5, respectively. (One can estimate these values from the ion-collection efficiency curves for $e^- + H_2$ collisions shown in Fig. 1(a) at H^+ energies near the distribution maxima in Fig. 2.)

Note that all these collection fractions are well below the 0.400 assumed by Rapp, Englander-Golden, and Briglia [1]. In fact, their (weighted) average is only 0.215, implying that the dissociative-ionization fraction measured by Rapp, Englander-Golden, and Briglia [1] should be increased by a multiplicative correction factor of $0.400/0.215 = 1.86$.

Similar calculations were made at other electron energies, yielding correction factors between about 1.6 and 1.7 for electron energies from 100–1000 eV, but increasing to 2.5 at 50-eV electron energy and to above 4.0 below 40 eV. We show these results in Fig. 7. The curve labeled A is the dissociative-ionization fraction reported by Rapp, Englander-Golden, and Briglia [1] [see their Fig. 4(a)], and curve B shows our correction of these data.

Note that below 32-eV electron energy, the correction factor exceeds 10. Here, most of the H^+ are from the low-energy peak 1 distribution not collected by Rapp, Englander-Golden, and Briglia [1]. Our estimated dissociative-ionization fraction for these H^+ (i.e., from the $^2\Sigma_g^+$ state of H_2^+) is shown by curve C in Fig. 7.

We have also included the recent results of Krishnakumar and Srivastava [3] in Fig. 7 for comparison. As can be seen, except for a limited electron-energy range around 250 eV, these results fall somewhat below our predictions. Furthermore, we know of no physical mechanism that could explain the abrupt change in slope exhibited by these results at 200-eV electron energy.

The absolute cross sections for each of the five processes yielding H^+ during $e^- + H_2$ collisions and the total H^+ production cross section are shown in Fig. 8. This latter cross section is simply the product of curve B in Fig. 7 and the total ionization cross section for H_2 from Rapp and Englander-Golden [2]. The individual partial cross sections come from such (area-under-the-curve) fractions as listed above for 75-eV electron energy times this total cross section for H^+ formation.

The reason we have presented these results in this way is to point out either a problem or a misconception on our part. The H^+ energy dependence of the partial cross section for peak 1 is fixed by Eq. (2) and the total H_2^+ production cross section, which falls off at high electron energies more or less with the $E_e^{-1} \ln E_e$ energy dependence expected for such an optically-allowed ionization process. In contrast, all the other partial cross sections shown in Fig. 8 fall off as E_e^{-1} at the higher electron energies, a dependence usually found for optically-

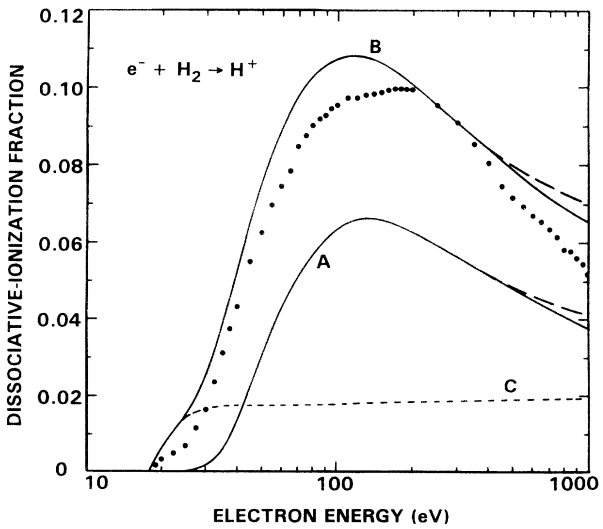

FIG. 7. Dissociative-ionization fractions for electron impact on H_2. Curve A shows the results of Rapp, Englander-Golden, and Briglia (Ref. [1]) and the data points are from Krishnakumar and Srivastava (Ref. [3]). Curve B shows our calculated correction of curve A, and curve C is our estimate of the H^+ fraction from the $^2\Sigma_g^+$ state of H_2^+.

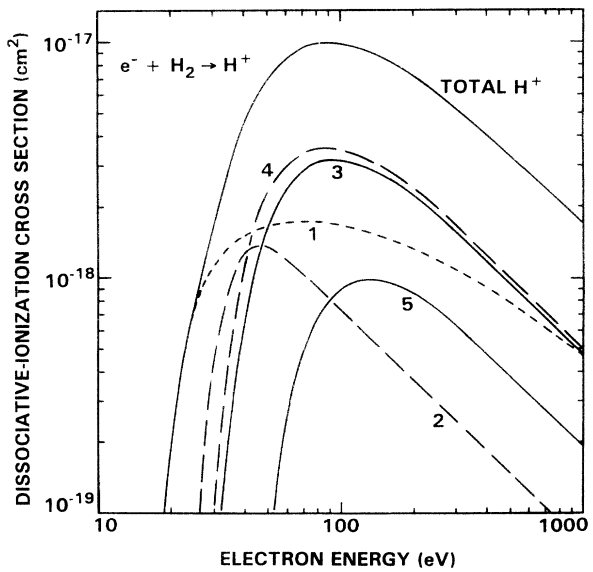

FIG. 8. Dissociative-ionization cross sections for electron impact on H_2 for each of the five modeled processes and the total H^+ production cross section.

disallowed processes. Yet the peak 4 process, direct excitation to the repulsive $^2\Sigma_u^+$ of H_2^+, should be allowed, as should at least the $H^+ + H^+$ contribution to peak 5, a seeming contradiction of our expectations.

It could perhaps be argued that the dissociative-ionization-fraction measured by Rapp, Englander-Golden, and Briglia [1] may be decreasing too fast at the larger electron energies. However, to obtain even the E_e^{-1} energy dependences of the partial cross sections in Fig. 8 for peaks 2–5, it was necessary to raise the high-electron-energy dependence of curve *B* in Fig. 7 to the long-dashed curve, which would then require a similar increase to curve *A*. There may be some justification for this adjustment, as the dissociative-ionization fraction measured for D_2 at the higher electron energies [33] appears to decrease approximately as this dashed-line curve, and these two reactions should behave similarly [1]. Clearly, however, to increase the high-electron-energy portions of curves *A* and *B* enough to cause the peak 4 cross section in Fig. 8 to decrease like $E_e^{-1}\ln E_e$ would require a much larger increase in the measured Rapp, Englander-Golden, and Briglia [1] data than seems plausible (to say nothing about the increased discrepancy with the measurements of Krishnakumar and Srivastava [3] that would result).

Another possible resolution of this difficulty might be that our peak 4 distribution is not actually the result of H^+ production from the dissociative $^2\Sigma_u^+$ state of H_2^+. Indeed, if these H^+ were the result of excitation of an optically-forbidden, doubly-excited state of H_2 followed by an autoionization (which process could be a contributor to peaks 2 and 3), such an E_e^{-1} electron-energy dependence might be reasonable. This would seem, however, to be in conflict with the current thinking about the source of these energetic H^+ from this reaction (as reflected in most of the H_2 references cited here).

Finally, one could ask if our calculations simply underestimate the required corrections to the Rapp, Englander-Golden, and Briglia [1] data at the higher electron energies. We could increase curve *B* in Fig. 7 relative to curve *A* by postulating the emergence of an additional source of low-energy H^+ at such higher electron energies. In addition to being unlikely, however, this would not increase the absolute contribution of peak 4 to the total H^+ production cross section, and thus not resolve the difficulty. Clearly additional study of this issue seems warranted.

The dissociative-ionization fractions for N_2 and O_2 targets are shown in Fig. 9, where curves *A* are again from the original data of Rapp, Englander-Golden, and Briglia [1] and curves *B* show our corrections of these results. The data points of Krishnakumar and Srivastava [4,5] shown here include small contributions from N^{2+} and O^{2+} to the N^+ and O^+ cross sections, these doubly-charged ions being weighted twice to be consistent with the energetic-atomic-ion currents measured by Rapp, Englander-Golden, and Briglia [1]. (The cross sections for N_2^{2+} and O_2^{2+} production from Märk [34] were used to separate the $N^+ + N_2^{2+}$ and $O^+ + O_2^{2+}$ cross sections actually given by Krishnakumar and Srivastava [4,5].

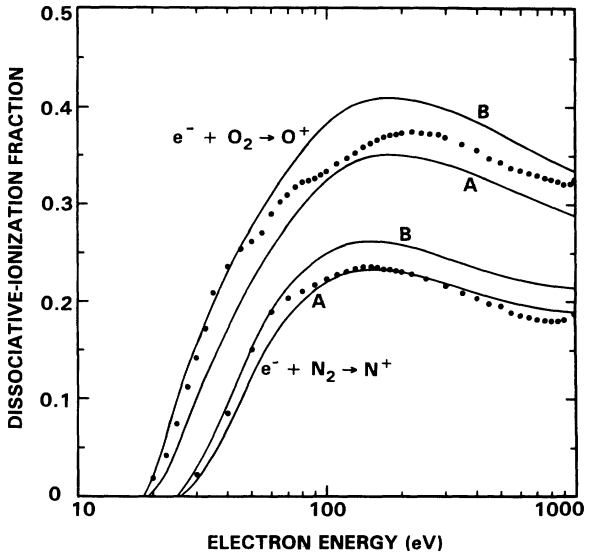

FIG. 9. Dissociative-ionization fractions for electron impact on N_2 and O_2. Curves *A* are the results of Rapp, Englander-Golden, and Briglia (Ref. [1]) and the data points are from Krishnakumar and Srivastava (Refs. [4] and [5]). Curves *B* show our calculated corrections of curves *A*.

For the most part, the data of Krishnakumar and Srivastava [4,5] again tend to lie below our curve *B* results, although the agreement is reasonably good at the lower electron energies. These data also show more structure than exhibited by curves *B*, and the apparent turn up of these fractions at electron energies close to 1000 eV seems physically improbable.

We will not here show plots of the individual partial cross sections for model peaks 1–10 for N^+ and O^+ formation as done for H^+ formation in Fig. 8 (although they are available upon request). However, to the extent that these partial cross sections have physical significance, the processes becoming important only at lower electron energies (peaks 3 and 6 for N^+ formation and 2, 4, and 6 for O^+ formation, the same peaks to which we assigned nonzero polarizations in Sec. III) exhibited similar electron-energy dependences to partial cross section 2 for H^+ formation in Fig. 8, reaching their maxima at low electron energies and decreasing rapidly thereafter. All other partial cross sections, however, exhibited rather broad maxima, and decreased less rapidly at the higher electron energies, certainly not inconsistent with an eventual $E_e^{-1}\ln E_e$ behavior. Thus the problem with the H_2 data discussed above does not appear to be present (or is at least not as serious) for N_2 and O_2 targets.

Our calculated curve *B* in Fig. 9 for O_2 averages to be about 17% above curve *A* for electron energies larger than 75 eV. More than half of these O^+ not collected by Rapp, Englander-Golden, and Briglia [1] are from the "zero-energy" O^+ peak (see Fig. 5). While the similar N^+ contribution is somewhat smaller, it is apparent that the data of Locht and his colleagues [15,16,31] upon

which our models of these zero-energy peaks are based, are crucial to the outcome of this study.

Locht and colleagues [15,16,31] do not describe uncertainties in their measurements except for the ion-energy-scale determinations made to deduce the sources of the atomic ions observed. However, Locht [35] has indicated that if the measured heights of these zero-ion-energy peaks are incorrect, they are "much more likely to be too small than too large" relative to the rest of the ion-energy distributions, as would occur if the apparatus had some unrecognized discrimination against very-low-energy ions [36].

If we arbitrarily double the relative magnitudes of peaks 1 in our model calculations for O_2 and N_2 molecules, curves *B* in Fig. 9 would increase by about 9% and 5%, respectively (again, for electron energies above 75 eV, below which larger increases would result). Similar increases (or decreases) in the relative magnitudes of the other peaks have much smaller effects, for the ion-collection fractions for more energetic O^+ [see Fig. 1(b)] or N^+ are much closer to the 40% value assumed by Rapp, Englander-Golden, and Briglia [1]. A similar argument explains why our calculations are rather insensitive to changes in the shapes or widths of these ion-energy-distribution peaks, their polarizations, or on their exact locations on the ion-energy scales used. Thus most of the uncertainties in these calculations stem from the lack of a more complete set of energy- and angular-distribution data at the lower ion energies. Nevertheless, we believe the corrections to the data of Rapp, Englander-Golden, and Briglia [1] suggested by curves *B* in Fig. 9 are reasonably accurate, but quite possibly conservative.

In contrast, the strong dependences on ion energy and polarization found for the ion-collection-efficiency data in Fig. 1(a) for H^+ from H_2 indicate that these results are far more sensitive to the model parameters used. In particular, at the lower electron energies where the (peak 2) experimental results [17,18] are in such conflict and the H^+ polarizations so large, the corrections made to the data of Rapp, Englander-Golden, and Briglia [1] must be considered quite approximate, although it is clear they must be large. At higher electron energies, however, where these autoionization processes simulated by peak 2 are less significant, the dominant uncertainty stems from the H^+ fraction assumed for curve *C* (peak 1) in Fig. 7 as obtained from Eq. (2). If the 0.021 value of $N(H^+)/N(H_2^+)$ found there (in the high-electron-energy limit) is assigned a reasonable uncertainty of ± 0.008, the corresponding uncertainty introduced in curve *B* in Fig. 7 is here about $\pm 10\%$.

In summary, we believe the dissociative-ionization fractions (and therefore, the dissociative-ionization cross sections) reported by Rapp, Englander-Golden, and Briglia [1] for electron impact on H_2, N_2, and O_2 molecules should be revised upward to account for the low-energy atomic ions not collected during the measurements. Particularly large corrections must be made for $e^- + H_2$ collisions, because of the experimental conditions under which these measurements were made. Our corrections to these Rapp, Englander-Golden, and Briglia [1] data generally yield larger dissociative-ionization fractions than those obtained from the data of Krishnakumar and Srivastava [3–5]. Additional studies of these important reactions are clearly needed to supplement the available data and to examine the electron-energy dependence of these ionization processes at the higher electron energies.

ACKNOWLEDGMENTS

The authors thank R. Locht for sending large copies of his N^+ and O^+ ion-energy-distribution data for our convenience, and S. Srivastava for providing tabulated H^+ and H_2^+ production cross sections prior to their publication. Comments by R. Van Brunt were of help in evaluating some of the available experimental data. This work was partially supported by the Aeronomy Program, Division of Atmospheric Sciences, National Science Foundation.

[1] D. Rapp, P. Englander-Golden, and D. D. Briglia, J. Chem. Phys. **42**, 4082 (1965).
[2] D. Rapp and P. Englander-Golden, J. Chem. Phys. **43**, 1464 (1965).
[3] E. Krishnakumar and S. K. Srivastava, J. Phys. B **27**, L1 (1994). A complete tabulation of these data will be published later.
[4] E. Krishnakumar and S. K. Srivastava, J. Phys. B **23**, 1893 (1990).
[5] E. Krishnakumar and S. K. Srivastava, Int. J. Mass Spectrom. Ion Phys. **113**, 1 (1992).
[6] Some dimensions and operating characteristics were obtained from D. Rapp (private communication).
[7] R. N. Zare, J. Chem. Phys. **47**, 204 (1967).
[8] R. J. Van Brunt, J. Chem. Phys. **60**, 3064 (1974).
[9] G. H. Dunn and L. J. Kieffer, Phys. Rev. **132**, 2109 (1963).
[10] L. J. Kieffer and G. H. Dunn, Phys. Rev. **158**, 61 (1967).
[11] K. Köllmann, Int. J. Mass Spectrom. Ion Phys. **17**, 261 (1975).
[12] R. J. Van Brunt, Phys. Rev. A **16**, 1309 (1977).
[13] J. A. D. Stockdale, V. E. Anderson, A. E. Carter, and L. Deleanu, J. Chem. Phys. **63**, 3886 (1975).
[14] R. J. Van Brunt and L. J. Kieffer, Phys. Rev. A **2**, 1293 (1970).
[15] R. Locht, J. Schopman, H. Wankenne, and J. Momigny, Chem. Phys. **7**, 393 (1975).
[16] R. Locht and J. Schopman, Int. J. Mass Spectrom. Ion Phys. **15**, 361 (1974).
[17] K. Köllmann, J. Phys. B **11**, 339 (1978).
[18] M. Landau, R. I. Hall, and F. Pichou, J. Phys. B **14**, 1509 (1981).
[19] M. D. Burrows, L. C. McIntyre, Jr., S. R. Ryan, and W. E. Lamb, Jr., Phys. Rev. A **21**, 1841 (1980).
[20] G. H. Dunn, Phys. Rev. Lett. **8**, 62 (1962).

[21] A. Crowe and J. W. McConkey, J. Phys. B **6**, 2088 (1973).
[22] G. H. Dunn, J. Chem. Phys. **44**, 2592 (1966).
[23] R. Browning and J. Fryer, J. Phys. B **6**, 364 (1973).
[24] M. R. Flannery, H. Tai, and D. L. Albritton, At. Data Nucl. Data Tables **20**, 563 (1977).
[25] Y. M. Chung, E. M. Lee, T. Masuoka, and J. A. R. Samson, J. Chem. Phys. **99**, 885 (1993).
[26] A. L. Ford, K. K. Doken, and A. Dalgarno, Astrophys. J. **195**, 819 (1975).
[27] H. Tai and M. R. Flannery, Phys. Rev. A **16**, 1124 (1977).
[28] R. J. Van Brunt and L. J. Kieffer, J. Chem. Phys. **63**, 3216 (1975).
[29] R. J. Van Brunt, G. M. Lawrence, L. J. Kieffer, and J. M. Slater, J. Chem. Phys. **61**, 2032 (1974).
[30] This may be a consequence of an interfering effect among the many possible dissociative-ionization channels available for these molecules. Where specific channels can be examined, nonzero polarizations above 50-eV electron energy are certainly possible. For example, see R. J. Van Brunt and L. J. Kieffer, J. Chem. Phys. **60**, 3057 (1974).
[31] J. Schopman and R. Locht, Chem. Phys. Lett. **26**, 596 (1974).
[32] L. J. Kieffer and R. J. Van Brunt, J. Chem. Phys. **46**, 2728 (1967).
[33] Rapp *et al.* (Ref. [1]) do not present data for D_2 in this paper even though measurements were made. However, their data can be found in L. J. Kieffer and G. H. Dunn, JILA Report No. 51, 1965 (unpublished).
[34] T. D. Märk, J. Chem. Phys. **63**, 3731 (1975).
[35] R. Locht (private communication).
[36] While the actual heights of these zero-ion-energy peaks could thus be larger than measured, the problem could be diminished somewhat by the contributions of potentially observable O_2^{2+} or N_2^{2+} ions to these peaks at electron energies above their thresholds. Locht and colleagues do not comment on this possibility, and we have ignored it in our analysis.